Journal of Marine Research, 62, 721–741, 2004

Observations of wind influence on exchange flows in a strait of the Chilean Inland Sea

by Arnoldo Valle-Levinson[1] and José Luis Blanco[1]

ABSTRACT

A >100-day time series of velocity profiles, sea level and wind velocity at a strait in the Chilean Inland Sea was analyzed to examine the effects of wind forcing on the mean two-layer exchange. Measurements took place in the Meninea Constriction of the Moraleda Channel during a period dominated by northerly winds. The mean flow in the strait, and in general in the Moraleda Channel, showed net surface northward outflow and net bottom southward inflow that likely resulted from the dynamical balance between pressure gradient and friction. The influence of tidal mixing on mean exchange flows was further suggested by isopycnals intersecting the bottom. The same momentum balance between pressure gradient and friction, applied with temporally varying sea level slopes, satisfactorily described the subtidal modifications to the mean exchange flows produced by wind forcing. The use of sea level slopes to explain the subtidal variability of velocity profiles at the Meninea Constriction was justified by the strong correlation between sea level slopes and wind stresses (0.84). In fact, the vertically integrated dynamics was essentially explained by the balance between wind stress and barotropic pressure gradient for northerly winds. Addition of bottom stress improved the dynamical explanation during periods of weak or southerly winds. This dynamical response was confirmed by the first two empirical orthogonal functions of the record. Two-layer exchange flows were weakened by northerly winds as depicted by the first empirical function mode, which was unidirectional throughout the water column in response to depth-integrated dynamics. The second empirical function mode was related to the depth-dependent response that followed the wind-induced sea level set-up.

1. Introduction

Exchange flows over sills and through constrictions dictate the water properties of the basins separated by such morphological features. The studies on exchange flows have established a hydraulic exchange two-layer theory that has been described in Farmer and Freeland (1983). Many of the studies on hydraulic exchange have been summarized by McClimans (1990) and by Bryden and Kinder (1991). Additional studies have focused on the modifications produced by barotropic forcing (e.g. Farmer and Armi, 1986; Hibiya and LeBlond, 1993; Helfrich, 1995). Despite the substantial body of literature on exchange flows, few efforts have studied the effects of wind forcing on such exchange (e.g. Murray

1. Center for Coastal Physical Oceanography, Ocean, Earth and Atmospheric Sciences Department, Old Dominion University, Norfolk, Virginia, 23529, U.S.A. ***email: arnoldo@ccpo.edu***

and Johns, 1997). In contrast to studies on barotropic forcing, the wind-induced flows are expected to be depth-dependent as the surface water moves with the wind and the bottom water moves against the wind (e.g. Wong, 1994). In particular, if the wind blows against the surface layer of the exchange flows, notable modifications should be expected. The purpose of this study is to document the wind-induced effects on the two-layer exchange at a channel constriction in the Chilean Inland Sea, the Meninea Constriction in the Moraleda Channel. Results show that wind forcing tends to disrupt the typical density-induced exchange flows.

Study area

The Moraleda Channel (Fig. 1) features two basins >200 m deep separated by the Meninea Constriction where the depth rises to 40–50 m and the width changes to ~2.5 km from 10–15 km. The constriction/sill restricts the exchange of waters at depths >50 m (Silva *et al.,* 1995). The water of the southern basin is less saline and more oxygenated than that of the northern basin. The deep water of the northern basin originates from the Equatorial Subsurface Water (Silva *et al.,* 1997). On the basis of hydrographic information, Silva *et al.* (1998) propose a conceptual two-layer exchange for the area of the Meninea Constriction. The less dense water flows northward at the surface and the denser water flows southward over the sill. The inflow through the Meninea Constriction allows the ventilation of the southern basin.

Tides in Moraleda Channel are mixed with semidiurnal dominance and maximum amplitude in spring tides of 2.8 m. During neap tides this amplitude decreases by approximately one half. The propagation of tidal waves in the channel region is in general southward with relatively weak influence from the small channels that extend westward to the Pacific Ocean (Fierro *et al.,* 2000). Wind forcing in the area exhibits well-defined seasonality. Northerly winds dominate in the spring and summer and tend to be weaker than winter winds that blow predominantly from the south. Sporadic spring/summer northerly winds can exceed 10–15 m/s (Cáceres *et al.,* 2002).

2. Data collection and processing

Time series of current velocity profiles, wind velocity and sea level were obtained at intervals of 10 minutes for more than three months from days 268 to 373 (September 25, 1998 to January 8, 1999) in the area of the Moraleda Channel in the Chilean Inland Sea. A total of six Conductivity-Temperature-Depth (CTD) casts (Fig. 1) were also obtained along the channel with a SeaBird SBE-19 CTD. These casts were carried out on November 28, 1998 (during the deployment) and on February 28, 1999 (~1.5 month after the end of the deployment). Additional CTD data obtained on October 29, 1995 at essentially the same locations were available for comparison. The CTD data were processed following customary protocol suggested by the instrument manufacturer to align sensors, derive variables and group them in bins, using the instrument software.

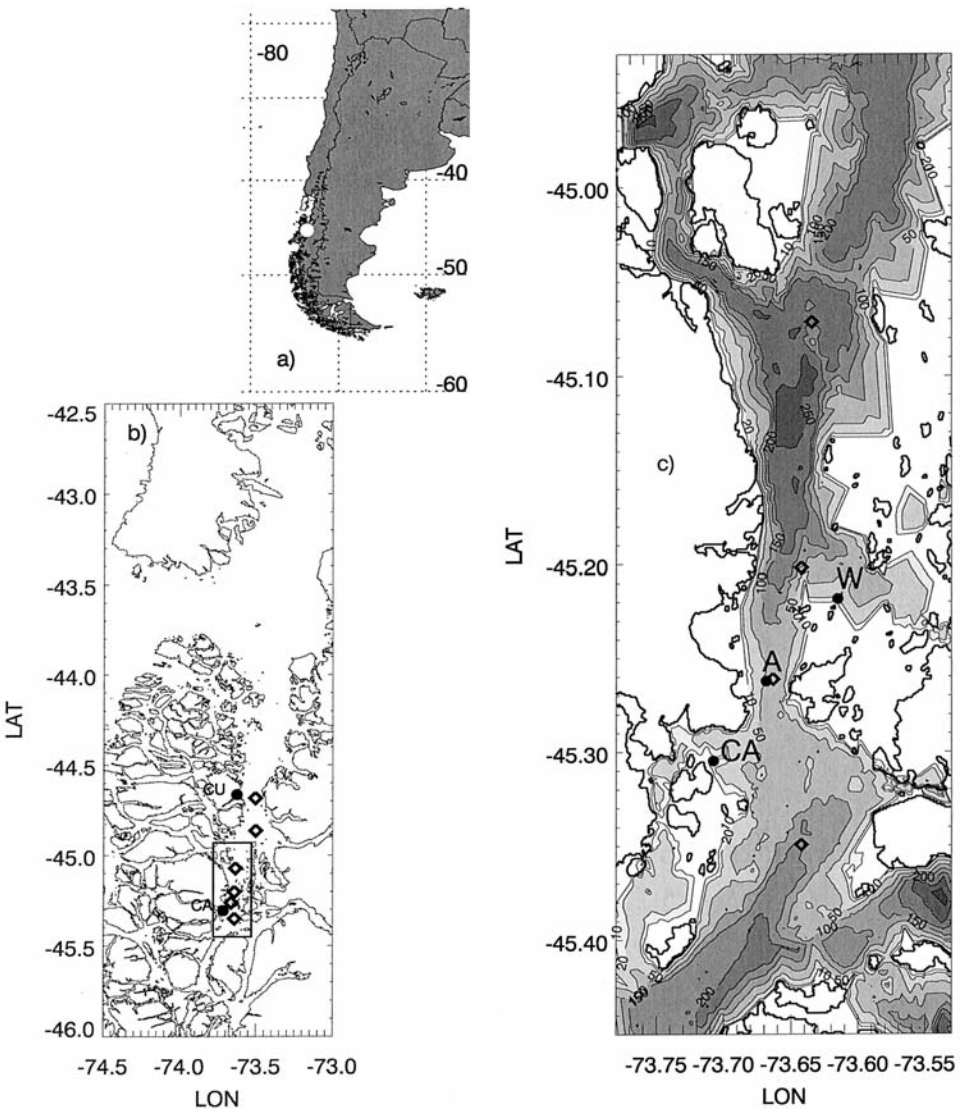

Figure 1. Study area in the context of (a) South America and (b) the Chilean Inland Sea. A zoom to the area in (c) shows bathymetry and the location of water (A for ADCP) and wind (W at Islote Rosas) velocity measurements, as well as the sea level (CA at Castillo and CU—only shown in (b)—at Cuptana) and CTD stations (diamonds, also shown in (b)). The Meninea Constriction spans from W to CA.

Time series of current velocity profiles were obtained with a RD Instruments 307.2 kHz acoustic Doppler Current Profiler (ADCP) between September 25, 1998 at 08:10 and January 8, 1999 at 14:30 local times. The instrument was deployed in the Meninea Constriction at 45.2622°S 73.6756°W ('A' on Fig. 1), pointing upward at ~4 m from the sea bed and over a depth of ~50 m. The ADCP recorded bins of 2 m at a rate of 30 pings per 10-minute ensemble, i.e., each recorded profile represented a 10-minute average of 20-second pings. The first and last usable bins were located at ~4 and ~34 m from the transducers, respectively. Bins close to the sea surface, typically one or two, were unusable because of side-lobe effects of sound propagating through the air-water interface.

Time series of sea level were recorded to the north (Cuptana, 'CU' on Fig. 1) and south (Castillo, 'CA' on Fig. 1) of the ADCP mooring. The record at Cuptana was obtained with an Aanderaa sensor at 44° 39.834′S, 73° 37.548′W, to the north of the constriction. The Castillo time series was recorded with an Ott Orpheous sensor at 45° 18.282′S, 73° 42.882′W, to the south of the constriction. Wind velocity was recorded at Islote Rosas ('W' on Fig. 1), at the northern end of the Meninea Constriction, with an Aanderaa AWS 2700 sensor.

All time series were smoothed with a Lanczos low-passed filter that had a half-power of 34 hours. This eliminated high frequency (greater than one cycle per day) variability. Although tidal influences on observed flows are presented, this study concentrates on the mean exchange flows through a strait in the Chilean Inland Sea and their subtidal variability, which was mostly produced by wind forcing.

3. Results

The general setting of the time series results is first established with a description of three hydrographic sections obtained in Canal Moraleda at different times of the year. This description allows direct interpretation of the mean flow profile observed at the Meninea Constriction. The subtidal variability of the water velocity profiles is then explored through the influence of fortnightly tidal forcing and wind forcing. The relative importance of tidal and wind-induced influences on the flow subtidal variability is explained on the basis of an essentially frictional momentum balance and through the presentation of the most relevant principal components (or empirical orthogonal function modes).

a. Hydrography

Profiles of temperature, salinity and density anomaly (sigma-*t*) obtained in 1995, and also during the deployment and 1.5 months afterward, showed that salinity and density increased toward the north in this area of the Chilean Inland Sea (Fig. 2). This was consistent with the source of oceanic water, found to the north at 'Boca del Guafo,' and the sources of fresh water located to the south at the head of the fjords and inlets (Silva *et al.,* 1998). It is noteworthy that in every distribution the slope of all isotherms, isohalines and isopycnals increased over the shallowest area that represents the Meninea Constriction

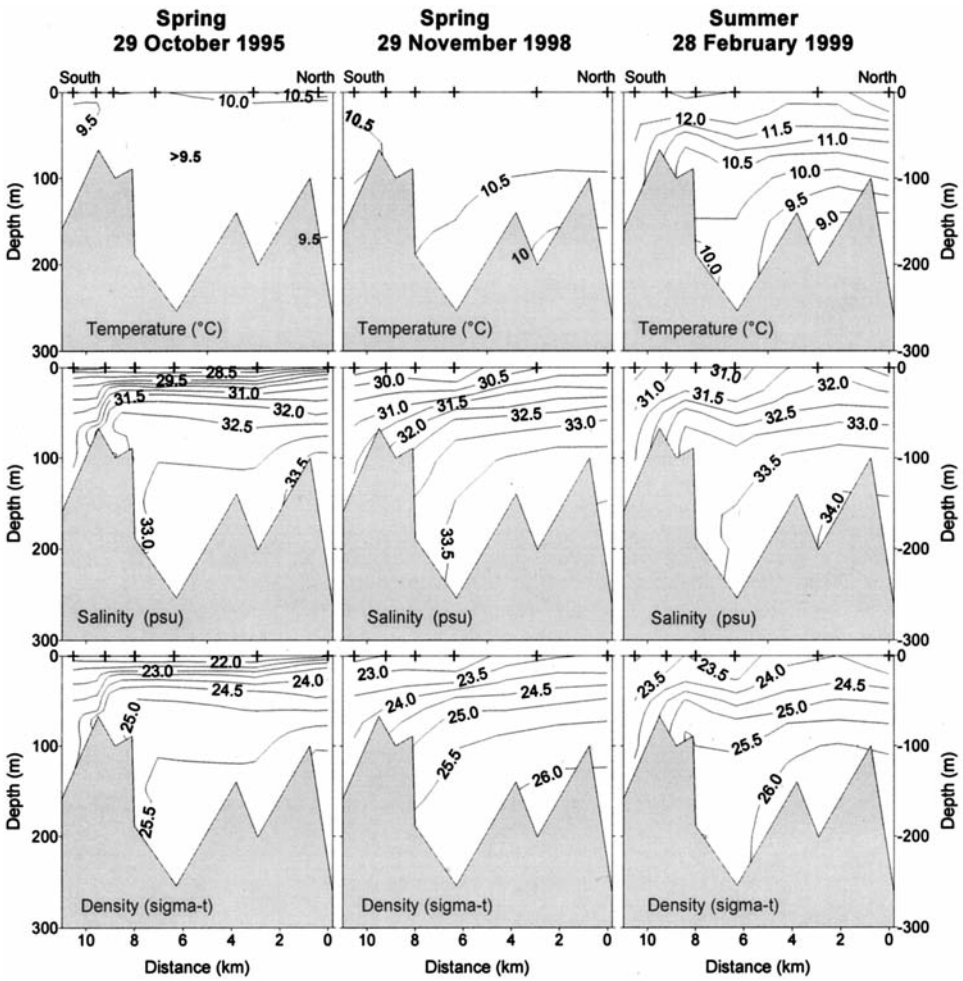

Figure 2. Along-channel sections of temperature, salinity and density anomaly in Moraleda Channel. Meninea Constriction appears between 8 and 10 km. Looking from east to west (north is on the right at 0 km).

(between 8 and 10 km in Fig. 2). This change in isolines slope produces asymmetric hydrographic distributions at either side of the constriction. Also, the change in slope suggests the influence of hydraulic effects that result from advective accelerations nearly balancing the pressure gradient. Additional influences from vertical mixing near the bottom are apparent from the isolines intersecting the bottom at sharp angles. This corresponds with theoretical expectations (e.g. Pratt, 1986; Johnson and Ohlsen, 1994) and observations in other environments (Valle-Levinson and Wilson, 1994). Also, vertical mixing effects are apparent from the vertical spread of isolines throughout the water column in contrast to the sharp pycnoclines observed elsewhere in the channels and inlets

of the region (e.g. Silva *et al.,* 1995). Increases in vertical mixing may represent subcritical conditions in the exchange flows relative to the propagation of an internal perturbation (e.g. Valle-Levinson *et al.,* 2001) or at least a reduction in exchange flows relative to inviscid hydraulic theory (Stenström, 2003). This frictional effect was first explored through the depiction of the mean exchange flows in the strait.

b. Mean flow

The mean flow profile obtained throughout the deployment period with the ADCP showed near-surface outflow (north-northeastward) and near-bottom inflow (south-southeastward) (Fig. 3a). This is the typical two-layer exchange flow expected for estuarine environments of this type and agreed with the hydrography acquired at different times of the year (Fig. 2). The magnitudes of the mean flows were extreme, close to 0.17 m/s, at the bins closest to the surface and bottom. These extreme values spread out over an angle of $\sim$150° and reflected mean flows that rotated clockwise from surface to bottom (Fig. 3a). The sense of rotation coincided with that of a bottom Ekman spiral in the southern hemisphere. However, the magnitude of the mean flows may not be explained with Ekman dynamics, which predicts decreasing magnitude with increasing depth. The mean flow observed indicated increased flow toward the bottom. Therefore, the veering of the mean flow with depth cannot be explained with Ekman dynamics. It appears that the mean flows were influenced by a force directed in the sense of the depth-averaged flow (dark and thick arrow in Fig. 3b) throughout the water column. Subtraction of the depth-averaged flow from the depth-dependent mean vectors produced a mean flow aligned with the main bathymetric orientation at Meninea Constriction. The force that affected the mean flows (represented by the depth-averaged flow) may have resulted from the lateral balance (aligned with an x axis) between barotropic pressure gradient and bottom friction:

$$g\,\frac{\partial \eta}{\partial x} = \frac{C_D U^2}{H} \tag{1}$$

where g, H, C_D, η, and U are the acceleration due to gravity (9.8 m/s^2), water column depth (50 m), nondimensional bottom drag (0.0025), sea surface elevation, and depth-averaged lateral flow, respectively. The observed depth-averaged flow U of 0.08 m/s could have been caused by a sea-surface slope ($\partial\eta/\partial x$) of $\sim 3 \times 10^{-8}$, which is relatively small and perhaps related to the channel's curvature. Notice that even though the mean lateral flow was unidirectional throughout the water column, it represented conditions only at one point in the channel's cross-section; mass balance should be achieved with the rest of the flow distribution in the section as shown by Kasai *et al.* (2000) and Valle-Levinson *et al.* (2003).

The profile of the mean flow and the along-channel sections of salinity and density suggested that the mean dynamic balance at the observation point should have been dominated by frictional effects from tidal forcing (speeds that exceed 1 m/s). These effects should have balanced the pressure gradient established by the sea level slope and density

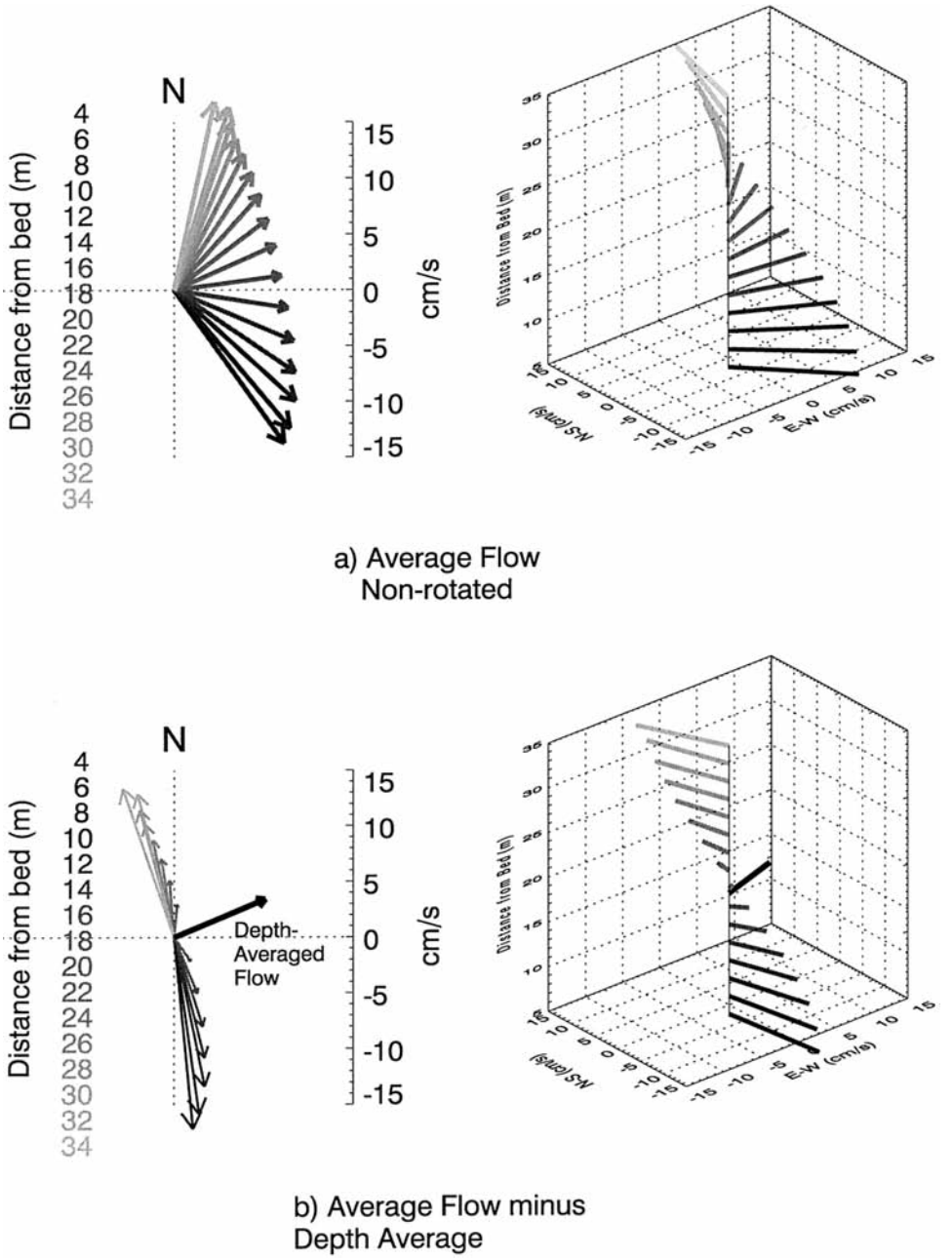

Figure 3. Various representations for the average velocity of the entire deployment illustrating near-surface outflow and near-bottom inflow. The grayscale of vectors represents distance from bed (m).

differences along the Inland Sea. In other words, the dynamics of the along-fjord (in the y direction) mean flow v could be represented as:

$$\frac{\partial^2 v}{\partial z^2} = -\frac{g}{A_z}\frac{\partial \eta}{\partial y} - \frac{g}{\rho A_z}\frac{\partial \rho}{\partial y} z \tag{2}$$

where A_z, ρ, and z are the vertical eddy viscosity (m^2/s), the water density (kg/m^3) and the vertical coordinate (positive upward), respectively. Integrating (2) twice under the assumption that the along-fjord density gradient is independent of depth, and applying the conditions $\partial u/\partial z = 0$ at the bottom ($z = -H$) and that the depth-integrated flow is zero (Officer, 1976), the solution adopts the following form:

$$v = -\frac{gH^3}{48\rho A_z}\left[11 + 24\frac{z}{H} - 8\left(\frac{z}{H}\right)^3\right]\frac{\partial \rho}{\partial y} - \frac{gH^2}{8A_z}\left[3 + 4\left(\frac{z}{H}\right)^2 + 8\frac{z}{H}\right]\frac{\partial \eta}{\partial y}. \tag{3}$$

Solution (3) would require prescription of both the slope $\partial\eta/\partial y$ and the density gradient $\partial\rho/\partial y$. It is customary to derive a dynamically consistent slope as a function of the density gradient so that v becomes only a function of the density gradient (e.g. Officer, 1976). The relationship between sea level and density gradients is obtained with the boundary condition that dictates a vertically integrated flow equal to the river discharge per unit width of estuary. Alternatively, the vertical integral of v may be made equal to zero because the result for only the density-induced flow remains unchanged. Here, an alternative approach was used in which the density gradient was defined in terms of the sea level slope using the no net vertically integrated v flow across the section, which yields:

$$\frac{\partial \rho}{\partial y} = -\frac{2\rho}{H}\frac{\partial \eta}{\partial y}. \tag{4}$$

This approach was used because the solution is later used to describe subtidal variations in flow by taking advantage of sea-level slope measurements along the study area. Substituting (4) into (3), the solution becomes:

$$v = \frac{gH^2}{12A_z}\left[1 - 6\left(\frac{z}{H}\right)^2 - 4\left(\frac{z}{H}\right)^3\right]\frac{\partial \eta}{\partial y} \tag{5}$$

which describes a mean flow profile with vertical structure given by a third order polynomial. The solution represents surface and bottom flows with the same magnitude but opposite signs and a zero mid-depth flow. The magnitude itself is sensitive to the water column depth as it is proportional to H^2. The observed profile of mean along-fjord flow showed an apparent constant vertical gradient throughout the water column (Fig. 4) and was remarkably similar to solution (5) with $\partial\eta/\partial y = 4 \times 10^{-7}$ (average slope throughout observation period) and $A_z = 2.5 \times 10^{-5}$ m^2/s (value yielding best fit with observed mean flow). The similarity of (5) with the observed mean flow indicated that the frictional balance (2) appropriately described the mean flow in the study area. This was consistent

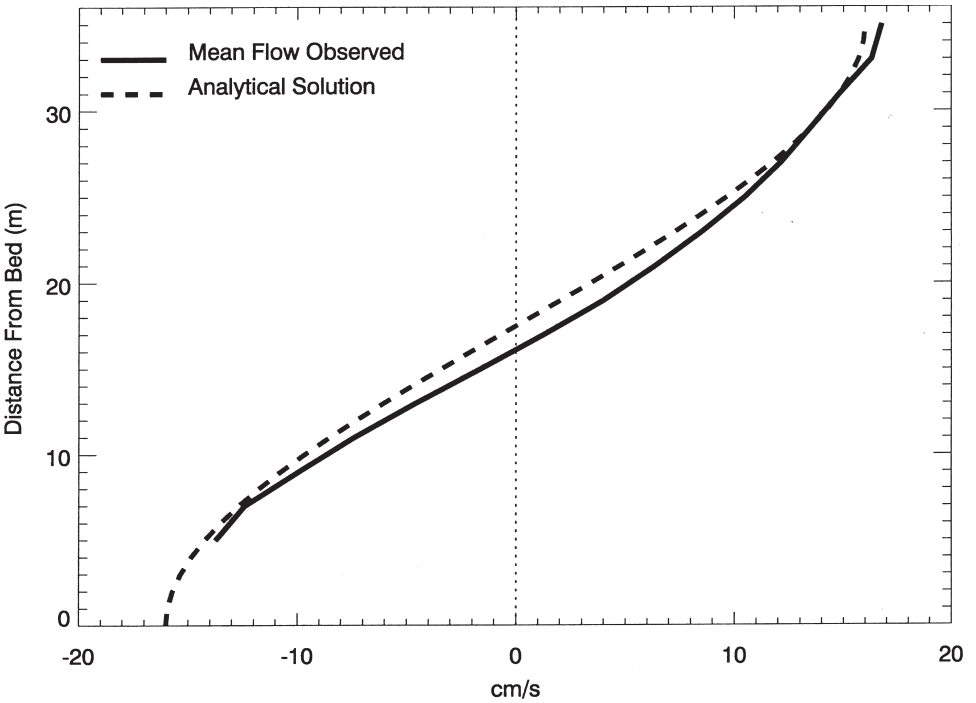

Figure 4. Observed mean flow for the entire deployment period compared to that predicted by analytical solution (5).

with the viscous advective diffusive (VAD) solution in which mixing, rather than the speed of internal waves, determines the horizontal velocity (Hogg *et al.,* 2001). The value of A_z that was needed to produce results similar to solution (5) was relatively small because it represented an average value through time and throughout a relatively deep water column. The same solution (5) is applied later to explain the subtidal variability of the along-channel flow. In order to assess such subtidal variability, the original observations had to be aligned to their principal axis, i.e., the axis of maximum variability.

c. Alignment of flow

The flow observations obtained with the ADCP showed different orientations for flood or ebb. Ebb flows were toward ~10°T and flood flows <40 cm/s were toward ~180°T (Fig. 5a). Interestingly, flood flows >40 cm/s were directed toward ~160°T. Strong flood flows were then affected by the morphology of Moraleda Channel (Fig. 1), apparently following the bathymetric orientation at the sampling site. Because of the observed changes in flow orientation, the direction of the principal axis of the flows was selected according to direction and magnitude (Fig. 5b). All ebb (northward) flows were rotated 10° counterclockwise whereas flood (southward) flows exceeding 40 cm/s were rotated 20°

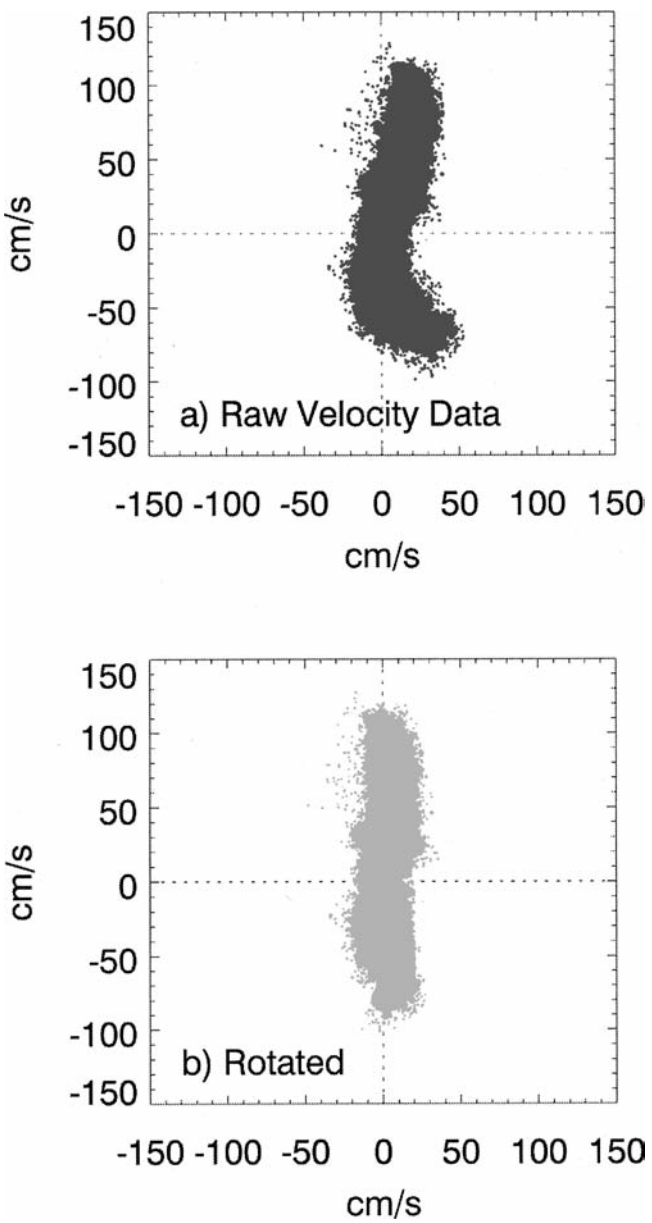

Figure 5. Alignment of all velocity data into along- and across-fjord components. (a) Ebb flows were toward ~10°T and flood flows >40 cm/s were toward ~160°T. (b) Ebb (northward) flows were rotated 10° counterclockwise whereas flood (southward) flows > 40 cm/s were rotated 20° clockwise.

clockwise. Weak flood flows (<40 cm/s) were left intact. These rotations allowed the definition of along-fjord flows v_a, positive seaward, and across-fjord flows u_a, positive toward the eastern flank of the channel.

d. Fortnightly variability

In order to examine tidal forcing effects on subtidal variability the mean flow profiles for both u_a and v_a as a function of tidal amplitude were determined. During periods of weak tidal ranges associated with neap tides, near-bottom inflows (negative) were stronger than during spring tides, but near-surface outflows (positive) were weaker in neap tides than in spring tides (Fig. 6a). The near-surface flows differed from the typical response of density-induced exchange flows that strengthen during neap tides in several estuaries (e.g. Haas, 1977; Nunes and Lennon, 1987; Griffin and LeBlond, 1990; Jay and Smith, 1990; Simpson *et al.,* 1990). Although the tidal currents in this system exceed 1 m/s in spring tides and decrease by nearly one half in neap tides, there was no apparent fortnightly modulation in the exchange flows. It is likely that wind forcing masked the fortnightly modulation in v_a expected from tidal forcing (as seen later in Figs. 7 and 8). In contrast, the across-fjord component u_a showed an increase in two-layer flow from neap to spring tides (Fig. 6b). The two-layered u_a flow featured westward (negative) flow at surface and eastward (positive) flow at depth, consistent with curvature effects (e.g. Geyer, 1993). The enhancement of u_a mean flows in spring tides was attributed to the increase in centrifugal accelerations that are proportional to tidal forcing (Chant, 2002). The main idea drawn from Figure 6 was that tidal forcing seemed to play a minor role in the subtidal variability of v_a but a non-negligible influence on u_a. The strongest influence on the subtidal variability of the flows was exerted by wind forcing as explained next.

e. Wind-induced variability

The low-passed v_a flow showed that water exchange (i.e. two-layer flow) was most robust during periods of weak wind forcing (Fig. 7), from days 315 to 325 and from days 345 to 357. During these periods of weak wind, the magnitude of net outflows/inflows exceeded that of the mean flow displayed in Figure 3 by almost 50% (Fig. 7b). Reversals of surface outflows or bottom inflows occurred only in a few occasions throughout the 103 days of the record (six examples featured on Fig. 7). These were occasions when wind forcing overwhelmed the baroclinic pressure gradient forcing as determined by the nondimensional Wedderburn number W (e.g. Monismith, 1986):

$$W = \frac{\tau_s L}{g \Delta \rho H_o^2}$$

where τ_s is the surface wind stress and L is the length of the basin (~90 km over the portion of the Moraleda Channel) and the other variables as defined before. For wind speeds of 10 m/s τ_s is 0.13 Pa (Large and Pond, 1981) and $W \sim 1$, i.e. the threshold for wind stress to overcome baroclinic influences.

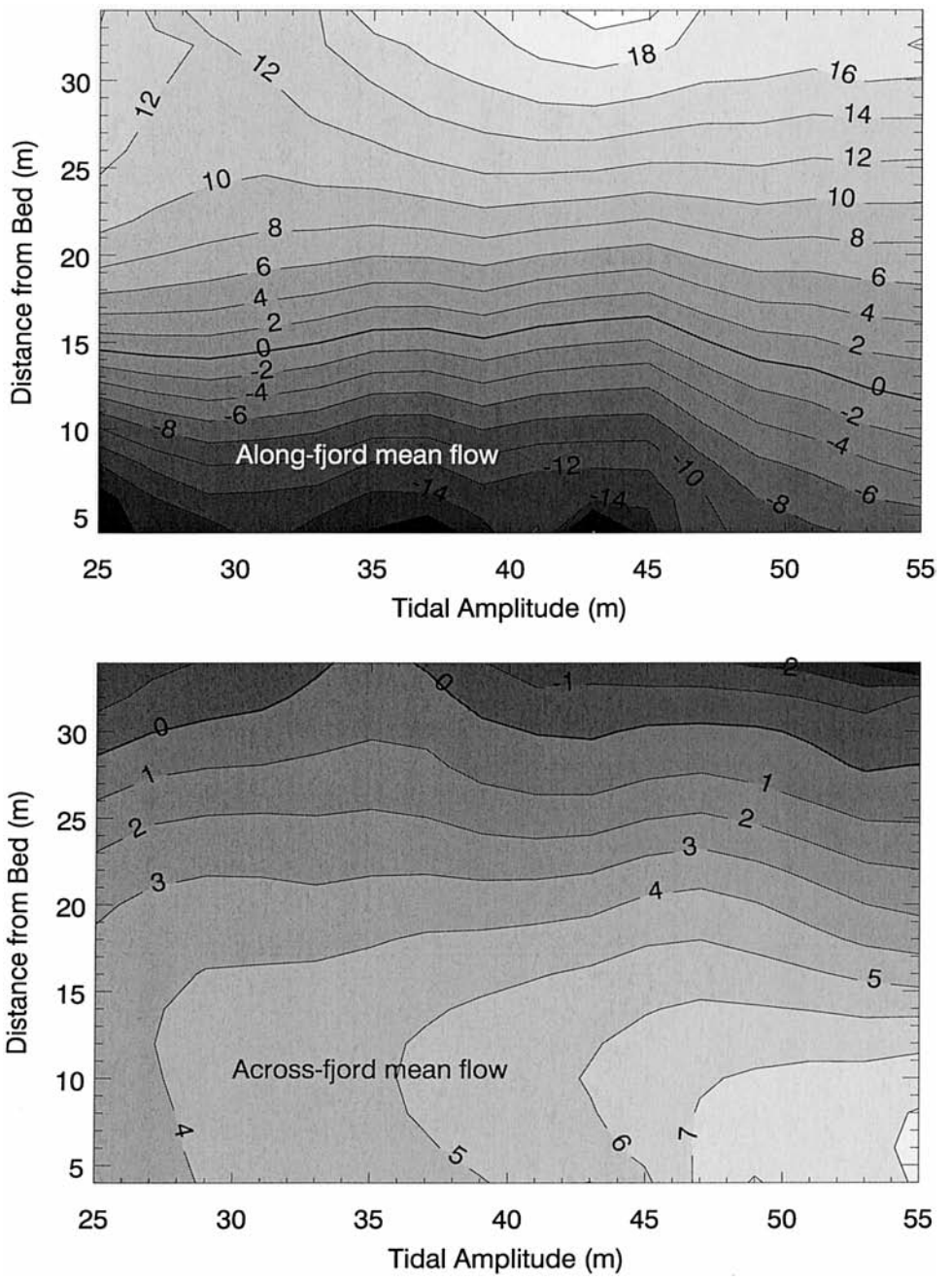

Figure 6. Mean flows as a function of tidal amplitude. Positive along-fjord flow is toward the ocean. Positive across-fjord flow is toward the eastern shore of the channel.

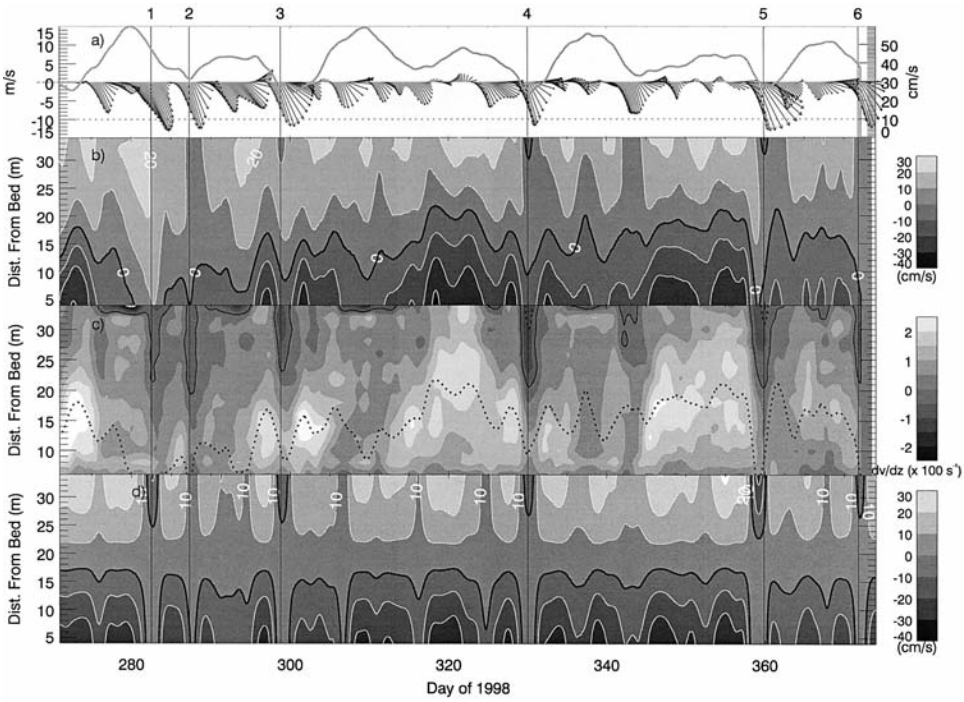

Figure 7. Low-passed variability of (a) wind and amplitude of tidal current (to denote spring and neap tides); (b) principal axis of flow (dark thick line is the zero contour); (c) vertical shear of the principal axis of the flow ($\times$ 100 s^{-1}; dotted contour is the interface between the two layers, which coincides with maximum shears; dark contour delineates regions of negative shears); and (d) subtidal variability derived from Eq. (5). Numbers 1–6 on top of the figure denote the northerly wind pulses that exceed 10 m/s ($W > 1$).

Episodes of outflow reversals (labeled 4, 5, and 6 on top of Fig. 7) coincided with weakening of near-bottom inflows and deepening of the interface between inflows and outflows. Analogous events (labeled 1, 2 and 3) exhibited bottom inflow reversal and surface outflow weakening. All these 6 events were related to the strongest pulses (>10 m/s, $W > 1$) of northerly wind. The six northerly wind pulses also caused a sign reversal of vertical shears in along-channel flow owing to reversal or weakening of near-surface outflow (Fig. 7c). These sign reversals in vertical shears extended from the surface to nearly mid-depth (Fig. 7c). In addition, the six events labeled in Figure 7 were identified as the most anomalous in terms of weakened inflows and weakened outflows. The flow responses during the six wind pulses were related to the fact that northerly winds opposed the density-induced surface layer outflow and built up a negative sea level slope (subtidal sea level decreasing northward) by driving water southward. The barotropic pressure gradient associated with this sea level slope drove a near-bottom flow that also opposed the density-induced near-bottom inflow. Therefore, northerly wind forcing produced a two-

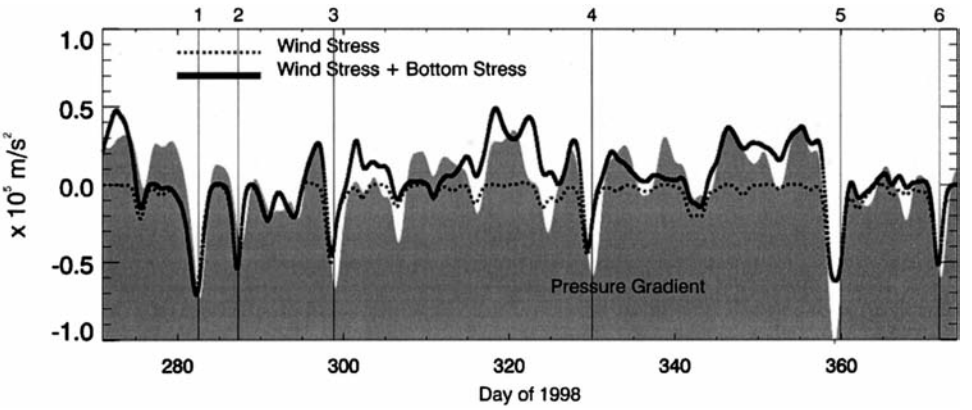

Figure 8. Contributions to the vertically averaged momentum balance ($\times 10^5$ m/s^2) shown in Eq. (6). The pressure gradient term is represented by the shaded area. Wind pulses >10 m/s are shown for reference. Local accelerations have negligible contributions and are not shown.

layer response that dampened the volume exchange through Meninea Constriction and may have even produced a weak three-layer exchange flow as in the last three pulses of the record (3, 4, 5 Fig. 7b): near-surface inflow (with the wind), interior outflow, and near-bottom inflow. This three-layer response to winds that oppose the density-induced near-surface outflow corresponds with observations (Svendsen and Thompson, 1978; Cáceres *et al.,* 2002) and numerical simulations (Klinck *et al.,* 1981) in other fjord systems.

Interestingly, five of the six northerly wind pulses occurred at or near neap tides, in close periodicity to the passage of atmospheric pressure systems over the study area. This coincidence of strong winds during neap tides may be fortuitous or it may in fact reflect a fortnightly/monthly modulation of atmospheric pressure that requires further scrutiny but which is beyond the scope of this study. An additional response to wind forcing that is worth noting was the variability of the interface depth between the two layers. Figure 7b shows that the changes of the interface, as given by the zero contour of the subtidal flows, followed closely the northerly component of the wind velocity, most notably during the strongest wind pulses. This data set showed that when the wind blew in the same direction as the net inflow (from north to south in this application) the interface of the exchange flow deepened. The deepening was a result of the dampening of net inflow by the wind-induced near-bottom outflow. Analogously, strong winds in the direction of net outflow should contribute to enhance the two-layer exchange. Winds from the south were weak in this time series and the response to this type of winds remains to be explored.

The wind-induced response contrasted with that expected from a barotropic tidal flow. Tidal forcing in general contributes to thicken the inflowing lower layer when it is in the direction of the net inflow, i.e., during flood periods (e.g. Farmer and Armi, 1988; Helfrich, 1995; Valle-Levinson *et al.,* 2001). In comparison, upfjord wind forcing caused the inflowing layer to become thinner and therefore the exchange hydrodynamics should be

different from that described in those studies dealing with barotropic forcing (pressure gradient mainly balanced by advection). This assertion is explored next through the frictional modifications to the mean flow given by solution (5).

f. Dominant hydrodynamics

Solution (5) for v_a, instead of v, was used to describe the variations from the mean observed profile produced by time-varying sea level slopes (instead of constant) measured between Cuptana (to the north, 'CU' in Fig. 1) and Castillo (to the south, 'CA' in Fig. 1), at a distance of 75 km. The observed subtidal variations of exchange flows (Fig. 7b) were reproduced reasonably well by the theoretical expectations portrayed by Eq. (5) for a value of A_z equal to 4.5×10^{-3} m^2/s (Fig. 7d). The relatively large value of A_z, compared to the value used in Figure 4, was necessary to produce the correct magnitude of predicted flows. The different values of A_z required in Figures 4 and 7d could indicate that advective processes, or that the temporal variability of mixing, contributed to the observed magnitude of exchange flows. The use of a constant A_z in space and time was an obvious source of discrepancy between observations and solution (5) because observations are expected to be influenced by different A_z associated with various forcings. Another disagreement between observations and analytical solution was the extent of the vertical excursions of the outflow/inflow interface (zero isotach). In the observations, this could have been related to the depth-independent wind-induced flow that set up the sea surface slopes or to advective effects, both of which were not included in solution (5). Nonetheless, the main features of v_a variations were consistent from observations to analytical results and suggested that subtidal exchange flows at the Meninea Constriction were mainly produced by the balance between pressure gradient and friction.

The overall resemblance between observations and analytical solution also indicated that the subtidal variations to the mean velocity profile could be adequately represented only with measurements of sea level slopes. Obviously, for this similarity to exist between theory and observations, the measured sea level slopes should reflect a dynamic consistency with the wind field. Otherwise, wind stress should be included explicitly in the analytical solution. In fact, the barotropic pressure gradient, which is proportional to the sea level slope, and the wind stress were highly correlated during the period of observations (Fig. 8). The correlation coefficient at zero lag was 0.77 and a maximum correlation coefficient of 0.85 was achieved at a lag of 8 hours, with the wind leading the pressure gradient. This high correlation further indicated that the vertically integrated dynamics responded to frictional influences that could be approximated with a linear momentum balance:

$$\frac{\partial \bar{v}_a}{\partial t} = -g\frac{\partial \eta}{\partial y} + \frac{\tau_{sy} - \tau_{by}}{\rho H} \tag{6}$$

where $\bar{v}_a$ is the vertically averaged along-fjord subtidal flow, and τ_{sy}, and τ_{by} are the surface stress and bottom stress, respectively. The surface stresses were calculated as in

Large and Pond (1981) and the bottom stresses were estimated as $\tau_{by} = \rho C_b v_b |V_b|$ using a nondimensional bottom drag coefficient C_b of 0.0025 and the near-bottom (bin closest to the bottom) along-fjord subtidal flow v_b and speed V_b. The neglect of advective accelerations in (6) is justified by the fact that they are at least one order of magnitude smaller than the terms on the right-hand side.

The terms in the momentum balance (6) were calculated with the information available from current profiles, wind measurements and sea level records (Fig. 8). The barotropic pressure gradient associated with the sea level slope between Cuptana and Castillo was represented by the shaded region of Figure 8. The entire period of observations was remarkably dominated by winds from the north (Fig. 7a). Northerly winds caused negative sea level slopes, i.e., water piling up from north to south. These negative sea level slopes were explained by the wind stress (negative τ_{sy}). The largest negative slopes corresponded to the six strongest wind pulses described in Figure 7. It is noteworthy that when sea level slopes were positive, the winds from the south (positive τ_{sy}) were not strong enough to balance the slopes (dotted line in Fig. 8). Then, for periods of southerly winds the inclusion of frictional effects through bottom stresses improved the match to the pressure gradient. Addition of local accelerations (term on the left-hand side of (6) and not drawn) produced insignificant improvements. This result indicated that sea level slopes responded to the frictional coupling between surface and bottom stresses and that the depth-integrated subtidal dynamics were mostly represented by a linear, frictional approach. This response was further examined with the estimation of empirical orthogonal functions (EOFs) associated with the along-channel velocity profile.

g. Empirical orthogonal functions

In this particular data set of velocity profiles as a function of time, the EOFs represent a linear combination of orthogonal modes with a vertical structure (Emery and Thomson, 1997). Time variations of the first EOF mode explained 56% of the subtidal variability of the along-channel flow (Fig. 9a) and were well-represented by the vertically averaged flow and the interface between subtidal inflows and outflows, i.e., the zero contour of Figure 7b. The vertical structure of this first mode showed the same sign throughout the water column, with a maximum at mid-depth and a minimum closest to the surface (right panel of Fig. 9a). This EOF structure suggested that most of the time (56%) the water column exhibited a unidirectional response to the forcing that caused subtidal variability. Most energetic unidirectional responses occurred, for example, on days 280, 295, 335, 340 (positive anomalies when multiplied by the 1st mode coefficients), and on days 317, 332, 349, 354 (negative anomalies when multiplied by the 1st mode coefficients). This was displayed in the temporal structure of the 1st EOF mode (Fig. 9a). For northerly wind, the unidirectional response translated into weakening of net inflows and strengthening of net outflows. The time variations of this first mode were also well represented by the accelerations resulting from the addition of wind stress and bottom stress (Fig. 10a), i.e. by depth-averaged frictional dynamics.

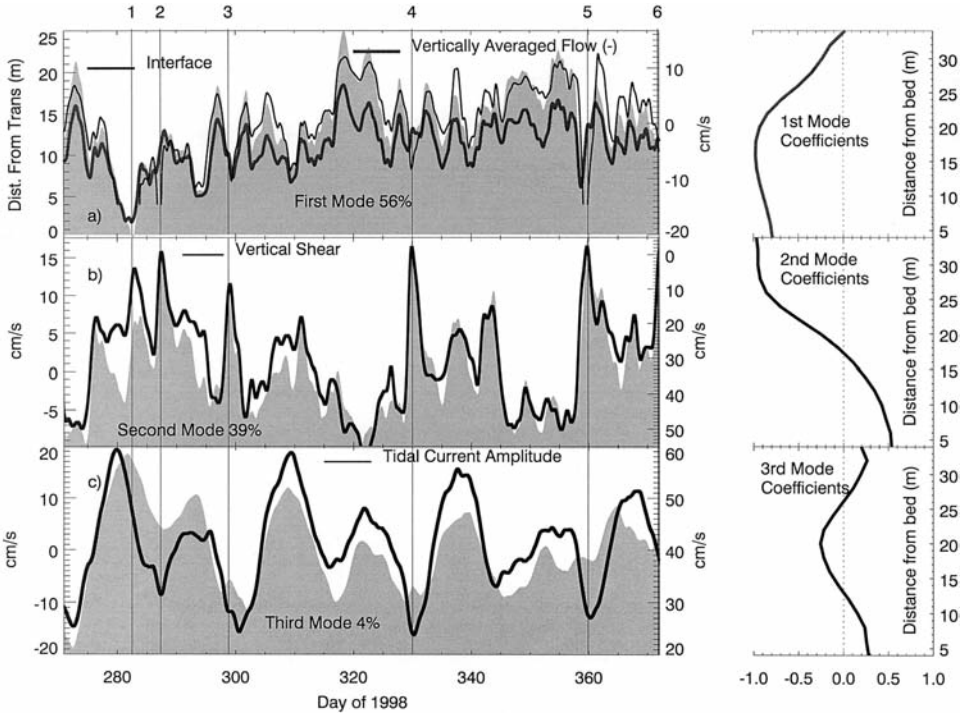

Figure 9. Temporal variations (left panels) and vertical structure (right panels) of the first 3 EOFs. On the left panels the EOFs temporal structure is represented by the shaded region of every panel. In the left panel of a), the left ordinate is for the depth of the interface, and the right ordinate is for the EOF mode and for the vertically averaged flow multiplied times −1. Wind pulses >10 m/s are shown for reference.

In turn, the time variations of the second mode explained a very important 39% of the subtidal variability of the along-channel flow (Fig. 9b). These variations were well-represented by the difference between near-surface and near-bottom subtidal flows (Fig. 9b) and related to the north component of the wind (Fig. 10b). The vertical distribution of the second mode exhibited a bidirectional structure that was apparent in several occasions. Clear two-layer responses to forcing ensued on days 277, 288, 299, 330, 360 (Fig. 9b) with negative anomalies at the surface and positive anomalies near the bottom. These represented hindered water exchange and mostly coincided with the strong northerly wind pulses. Analogously, positive anomalies at surface and negative anomalies at depth, indicating enhanced exchange, appeared for instance on days 322 and 351 (Fig. 9b) during periods of very weak winds. Together, the first and second modes explained 95% of the variability that portrayed a one- or two-layer response of the system to wind forcing. This response was satisfactorily explained by the dynamics represented by (2) with analytical solution (5). The combination of EOF Modes 1 and 2 suggested that the response of the water column at Meninea to strong wind forcing (>10 m/s) was initially

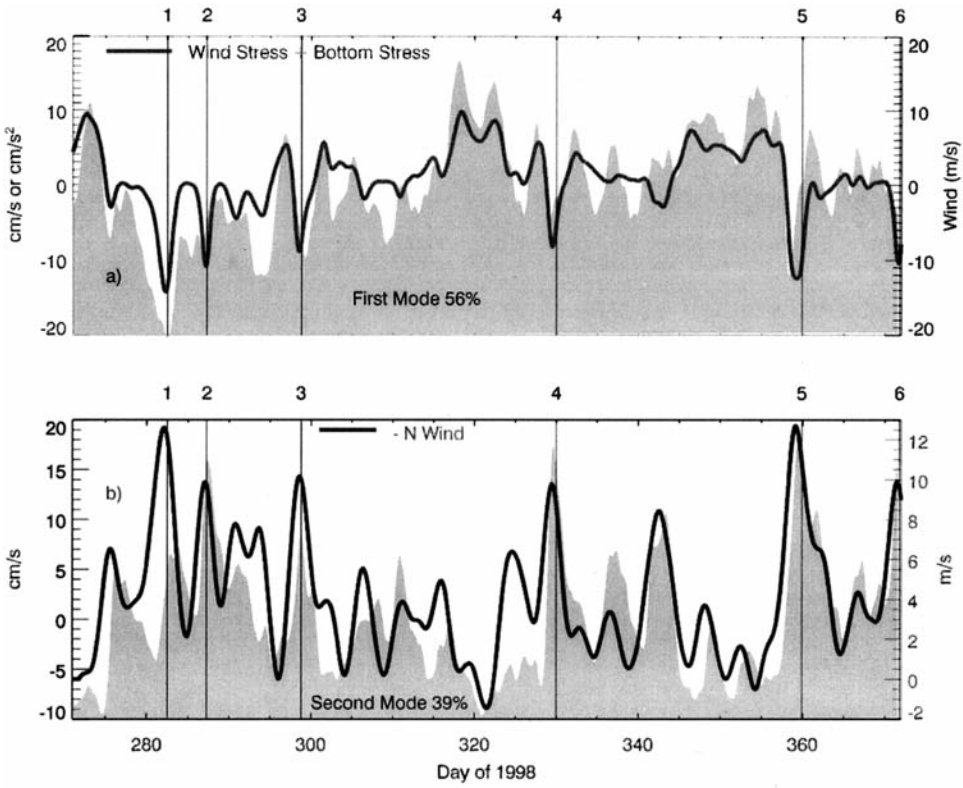

Figure 10. Relation between the first two EOF modes and physical forcing. Wind pulses >10 m/s are shown for reference. In b) the N wind component has been multiplied times −1.

unidirectional through downwind transport of water. Subsequently, the response changed to bidirectional after the establishment of the barotropic pressure gradient that drove upwind flow in the lower layer. Furthermore, weak winds tended to produce bidirectional responses in the water column. Even though these EOF modes are statistical, rather than physical, they are related to physical mechanisms related to the observed flows.

Finally, the third EOF mode explained only 4% of the variability and exhibited temporal variations that were correlated with the spring-neap tidal cycle (Fig. 9c). The vertical structure of the third mode consisted of a weak three-layered response. For example negative anomalies from the mean were displayed at surface and bottom on days 301 and 329, shown as negative values in the time series of Figure 9c. Positive anomalies at surface and bottom appeared, for example, on days 310 and 368 (Fig. 8c).

3. Conclusions

The information presented here constitutes another example that illustrates the fact that wind forcing may significantly modify the two-layer exchange through a channel constric-

tion or over a sill. The mean flow obtained in a shallow strait separating two basins of the Chilean Inland Sea indicated the presence of exchange flows that were consistent with the typical estuarine circulation. These mean exchange flows were driven by the pressure gradient that arose from the interaction between fresh and oceanic waters and were modified by frictional effects from tidal and wind forcing.

Tidal currents exceeded 1 m/s in spring tides and mostly affected the mean flow. Wind forcing produced variations of synoptic periodicity (2–7 days) that could appreciably modify the mean exchange flow. Strong wind ($>$10 m/s) for which the Wedderburn number $W > 1$ and that blew in the direction of the lower layer inflow hampered the two-layer exchange. In some cases, the initial response was downwind flow throughout the water column and the establishment of a barotropic pressure gradient represented by an upward sloping sea level toward the south. The subsequent response to this sea level slope occurred a few hours later as an upwind flow near the bottom, which translated into bidirectional wind-induced flows that opposed the mean estuarine exchange. The modifications to the mean exchange flows produced by observed northerly winds implied reduced flushing of the Chilean Inland Sea, south of the Meninea Constriction, during the wind episodes but enhanced flushing after the winds subsided. Therefore, it is suggested that wind forcing plays a pivotal role in the health of the system.

Wind-induced variability at the Meninea Constriction was well approximated through sea-level slope variations prescribed to an analytical solution obtained by the balance between pressure gradient and friction. The linkage between sea level slopes and wind stresses was confirmed by relatively simple depth-averaged dynamics. Wind forcing $>$10 m/s ($W > 1$) blowing in the opposite direction, northward, was not observed in this period but should enhance the two-layer exchange. The observations portrayed in this study also represented another example that illustrates the theoretical result where surface water flows in the direction of the wind and bottom water flows in the opposite direction (e.g. Wong, 1994).

Acknowledgments. This data set was collected as part of the project CIMAR-FIORDO 4 funded by the Chilean National Oceanographic Committee (CONA). The logistical support from the Hydrographic and Oceanographic Service of the Chilean Navy is greatly appreciated. AVL was funded by US NSF grant no. OCE-9812206. The comments of three anonymous reviewers are greatly appreciated. This work contributes to the scientific agenda of the Eastern Pacific Cosortium of the Inter-American Institute for Global Change Research (EPCOR-IAI).

REFERENCES

Bryden, H. L. and T. H. Kinder. 1991. Recent progress in strait dynamics. Rev. Geophys., *29,* 617–631.

Cáceres, M., A. Valle-Levinson, H. Sepúlveda and K. Holderied. 2002. Transverse variability of flow and density in a Chilean fjord. Cont. Shelf. Res., *22,* 1683–1698.

Chant, R. J. 2002. Secondary circulation in a region of flow curvature: relationship with tidal forcing and river discharge. J. Geophys. Res., *10.1029/2001JC001082.*

Emery, W. J. and R. E. Thomson. 1998. Data Analysis Methods in Physical Oceanography, Elsevier Science Inc., First Edition, 634 pp.

Farmer, D. M. and L. Armi. 1988. The flow of Atlantic water through the Strait of Gibraltar. Prog. Oceanogr., *21,* 1–105.

—— 1986. Maximal two-layer exchange over a sill and through the combination of a sill and contraction with barotropic flow. J. Fluid Mech., *164,* 53–76.

Farmer, D. M. and H. J. Freeland. 1983. The physical oceanography of fjords. Prog. Oceanogr., *12,* 147–220.

Fierro, J., M. Bravo and M. Castillo. 2000. Characterization of the tidal regime and currents along the Moraleda Channel (in Spanish). Cienc. Tecnol. Mar, *23,* 3–14.

Geyer, W. R. 1993. Three-dimensional tidal flow around headlands. J. Geophys. Res., *98(C1),* 955–966.

Griffin, D. A. and P. H. LeBlond. 1990. Estuary-ocean exchange controlled by spring-neap tidal mixing. Estuar. Coast. Shelf Sci., *30,* 275–305.

Haas, L. W. 1977. The effect of the spring-neap tidal cycle on the vertical salinity structure of the James, York and Rappahanock rivers, Virginia, USA. Estuar. Coast. Shelf Sci., *5,* 485–496.

Helfrich, K. R. 1995. Time-dependent two-layer hydraulic exchange flows. J. Phys. Oceanogr., *25,* 359–373.

Hibiya, T. and P. H. LeBlond. 1993. The control of fjord circulation by fortnightly modulation of tidal mixing processes. J. Phys. Oceanogr., *23,* 2042–2052.

Hogg, A. M., G. N. Ivey and K. B. Winters. 2001. Hydraulics and mixing in controlled exchange flows. J. Geophys. Res., *106(C1),* 959–972.

Jay, D. A. and J. D. Smith. 1990. Circulation, density distribution and neap-spring transitions in the Columbia River Estuary. Prog. Oceanogr., *25,* 81–112.

Johnson, G. C. and D. R. Ohlsen. 1994. Frictionally modified rotating hydraulic channel exchange and ocean outflows. J. Phys. Oceanogr., *24,* 66–77.

Kasai, A., A. E. Hill, T. Fujiwara, and J. H. Simpson. 2000. Effect of the earth's rotation on the circulation in regions of freshwater influence. J. Geophys. Res., *105,* 16,961–16,969.

Klinck, J. M., J. O'Brien and H. Svendsen. 1981. A simple model of fjord and coastal circulation interaction. J. Phys. Oceanogr., *11,* 1612–1626.

Large, W. G. and S. Pond. 1981. Open-ocean momentum flux measurements in moderate to strong winds. J. Phys. Oceanogr., *11,* 324–336.

Monismith, S. 1986. An experimental study of the upwelling response of stratified reservoirs to surface shear stress. J. Fluid. Mech., *171,* 407–439.

McClimans, T. A. 1990. Role of laboratory experiments and models in the study of sea strait processes, *in* The Physical Oceanography of Sea Straits, L. J. Pratt, ed., Kluwer Academic, Hingham, MA, 373–388.

Murray, S. P. and W. Johns. 1997. Direct observations of seasonal exchange through the Bal el Mandab Strait. Geophys. Res. Lett., *24,* 2557–2560.

Nunes, R. A. and G. W. Lennon. 1987. Episodic stratification and gravity currents in a marine environment of modulated turbulence. J. Geophys. Res., *92,* 5465–5480.

Officer, C. B. 1976. Physical Oceanography of Estuaries and Associated Coastal Waters, John Wiley, NY, 457 pp.

Pratt, L. J. 1986. Hydraulic control of sill flow with bottom friction. J. Phys. Oceanogr., *16,* 1970–1980.

Silva, N., C. Calvete and H. Sievers. 1997. Physical and chemical features of southern Chilean inlets between Puerto Montt and laguna San Rafael (Cimar-Fiordo I Cruise) (in Spanish). Cienc. Tecnol. Mar, *20,* 23–106.

—— 1998. Water masses and general circulation patterns of some of the southern chilean inlets between Puerto Montt and laguna San Rafael (Cimar-Fiordo I Cruise). (in Spanish). Cienc. Tecnol. Mar, *21,* 17–48.

Silva, N., H. Sievers and R. Prado. 1995. Oceanographic description of Chilean austral channel (41°S–46°S) (in Spanish). Rev. Biol. Mar. Valparaiso, *30,* 207–254.

Simpson, J. H., J. Brown, J. P. Matthews and G. Allen. 1990. Tidal straining, density currents and stirring in the control of estuarine stratification. Estuaries, *12,* 125–132.

Stenström, P. 2003. Mixing and recirculation in two-layer exchange flows. J. Geophys. Res., *108(C8),* 3526,doi:10.1029/2002JC001696.

Svendsen, H. and R. Thompson. 1978. Wind driven circulation in a fjord. J. Phys. Oceanogr., *8,* 703–712.

Valle-Levinson, A., F. Jara, C. Molinet and D. Soto. 2001. Observations of intratidal variability of flows over a sill/contraction combination in a Chilean fjord. J. Geophys. Res., *106(C4),* 7,051–7,064.

Valle-Levinson, A., C. Reyes and R. Sanay. 2003. Effects of bathymetry, friction and rotation on estuary-ocean exchange. J. Phys. Oceanogr., *33,* 2375–2393.

Valle-Levinson, A. and R. E. Wilson. 1994. Effects of sill bathymetry, oscillating barotropic forcing and vertical mixing on estuary/ocean exchange. J. Geophys. Res., *99(C3),* 5149–5169.

Wong, K. C. 1994. On the nature of transverse variability in a coastal plain estuary. J. Geophys. Res., *99(C7),* 14,209–14,222.

Received: *2 September, 2003;* revised: *3 August, 2004.*